8-10-2013

Determination of the Intrinsic Luminosity Time Correlation in the X-Ray Afterglows of Gamma-Ray Bursts

Maria Giovanna Dainotti

Vahe' Petrosian

Jack Singal
University of Richmond, jsingal@richmond.edu

Michal Ostrowski

Recommended Citation

Dainotti, Maria Giovanna, Vahe' Petrosian, Jack Singal, and Michal Ostrowski. "Determination of the Intrinsic Luminosity Time Correlation in the X-Ray Afterglows of Gamma-Ray Bursts." *The Astrophysical Journal* 774, no. 2 (August 10, 2013): 157. doi:10.1088/0004-637X/774/2/157.

The Astrophysical Journal, 774:157 (9pp), 2013 September 10 doi:10.1088/0004-637X/774/2/157

DETERMINATION OF THE INTRINSIC LUMINOSITY TIME CORRELATION IN THE X-RAY AFTERGLOWS OF GAMMA-RAY BURSTS

Maria Giovanna Dainotti[1,2], Vahe' Petrosian[1], Jack Singal[1,3], and Michal Ostrowski[1]
[1] Department of Physics & Astronomy, Stanford University, Via Pueblo Mall 382, Stanford, CA 94305-4060, USA; mdainott@stanford.edu, vahep@stanford.edu, jacks@slac.stanford.edu
[2] Obserwatorium Astronomiczne, Uniwersytet Jagielloński, ul. Orla 171, 31-501 Kraków, Poland; dainotti@oa.uj.edu.pl, mio@oa.uj.edu.pl
[3] Physics Department, University of Richmond, 28 Westhampton Way, Richmond, VA 23173, USA
Received 2012 December 26; accepted 2013 July 3; published 2013 August 26

ABSTRACT

Gamma-ray bursts (GRBs), which have been observed up to redshifts $z \approx 9.5$, can be good probes of the early universe and have the potential to test cosmological models. Dainotti's analysis of GRB *Swift* afterglow light curves with known redshifts and a definite X-ray plateau shows an anti-correlation between the rest-frame time when the plateau ends (the plateau end time) and the calculated luminosity at that time (or approximately an anti-correlation between plateau duration and luminosity). Here, we present an update of this correlation with a larger data sample of 101 GRBs with good light curves. Since some of this correlation could result from the redshift dependences of these intrinsic parameters, namely, their cosmological evolution, we use the Efron–Petrosian method to reveal the intrinsic nature of this correlation. We find that a substantial part of the correlation is intrinsic and describe how we recover it and how this can be used to constrain physical models of the plateau emission, the origin of which is still unknown. The present result could help to clarify the debated nature of the plateau emission.

Key words: cosmological parameters – gamma-ray burst: general – radiation mechanisms: non-thermal

Online-only material: color figures, machine-readable table

1. INTRODUCTION

Gamma-ray bursts (GRBs) are the farthest sources, seen up to redshift $z = 9.46$ (Cucchiara et al. 2011), and if emitting isotropically they are also the most powerful (with $E_{\rm iso} \leqslant 10^{54}$ erg s^{-1}) objects in the universe. In spite of the great diversity of their prompt emission light curves and their broad range spanning over seven orders of magnitude of $E_{\rm iso}$, some common features have been identified from the investigation of their afterglow light curves. A crucial breakthrough in this field was the observation of GRBs by the *Swift* satellite, which provides a rapid follow-up of the afterglows in several wavelengths, revealing a more complex behavior of the X-ray light curves than the broken power law generally observed before (O'Brien et al. 2006; Sakamoto et al. 2007). The *Swift* afterglow light curves manifest several segments. The second segment, when it is flat, is called the plateau emission. A significant step forward in determining common features in the afterglow light curves was made by fitting them with an analytical expression (Willingale et al. 2007, hereafter W07).

This provides the opportunity to look for universal features that could provide a redshift-independent measure of the distance, as in studies of correlations between the GRB isotropic energy and the peak photon energy of the νF_ν spectrum $E_{\rm iso}$–$E_{\rm peak}$ (Lloyd & Petrosian 1999; Amati et al. 2009), the beamed total energy E_γ–$E_{\rm peak}$ (Ghirlanda et al. 2004, 2006), L–V luminosity–variability (Norris et al. 2000; Fenimore & Ramirez-Ruiz 2000), L–$E_{\rm peak}$ (Yonekotu 2004), and possibly others (Schaefer 2003). The impact of detector thresholds on cosmological standard candles has also been considered (Shahmoradi & Nemiroff 2009; Petrosian 1998, 1999, 2002; Cabrera et al. 2007). Unfortunately, because of the large dispersion (Butler et al. 2009; Yu et al. 2009) and the absence of good calibration, none of these correlations allow the use of GRBs as "standard candles" as has been done, e.g., with Type Ia supernovae.

Dainotti et al. (2008, 2010), using the W07 phenomenological law for the light curves of long GRBs, discovered a formal anti-correlation between the X-ray luminosity at the end of the plateau, L_X, and the rest-frame plateau end time, $T_a^* = T_a^{\rm obs}/(1+z)$ (hereafter LT), described as

$$\log L_X = \log a + b \log T_a^*, \quad (1)$$

where T_a^* is in seconds and L_X is in erg s^{-1}. The normalization and the slope parameters a and b are constants obtained using the D'Agostini fitting method (D'Agostini 2005). Dainotti et al. (2011a) attempted to use the LT correlation as a possible redshift estimator, but the paucity of the data and the scatter prevents a definite conclusion, at least for a sample of 62 GRBs. In addition, a further step toward better understanding the role of the plateau emission was made with the discovery of new significant correlations between L_X and the mean luminosities of the prompt emission, $\langle L_{\gamma,\rm prompt}\rangle$ (Dainotti et al. 2011b).

The LT anti-correlation is also a useful test for theoretical models such as the accretion models (Cannizzo & Gehrels 2009; Cannizzo et al. 2011), the magnetar models (Dall'Osso 2010; Bernardini et al. 2012a, 2012b; Rowlinson et al. 2013; O'Brien & Rowlinson 2012), the prior emission model (Yamazaki 2009), the unified GRB and active galactic nucleus model (Nemmen et al. 2012), and the fireshell model (Izzo et al. 2013). Furthermore, it has also been recovered within other observational correlations (Ghisellini 2008; Sultana et al. 2012; Qi & Lu 2012). Finally, it has been applied as a cosmological tool (Cardone et al. 2009, 2010; Postnikov et al. 2013). Here, we study an updated sample of 101 GRBs and investigate whether the LT correlation is intrinsic or induced by the cosmological evolution of L_X and T_a^*, and/or observational biases due to the instrumental threshold. This step is necessary to cast light on the nature of the plateau emission, to provide further constraints on the theoretical models, and possibly to assess the use of the LT correlation as a model discriminator. In Section 2, we describe the data and the results from a correlation test carried out using

the raw data. In Section 3, we use the EP method to determine the intrinsic correlation between L_X and T_a^*. In Section 4, the cumulative density and luminosity are defined and derived. This is followed by a discussion section.

2. LIGHT CURVE DATA AND RAW CORRELATIONS

We have analyzed the sample of all GRB X-ray afterglows with known redshifts detected by *Swift* from 2005 January up to 2011 May for which the light curves include early X-ray data and therefore can be fitted by the W07 model. Willingale proposed a functional form for $f(t)$:

$$f(t) = \begin{cases} F_i \exp\left(\alpha_i \left(1 - \frac{t}{T_i}\right)\right) \exp\left(-\frac{t_i}{t}\right) & \text{for } t < T_i \\ F_i \left(\frac{t}{T_i}\right)^{-\alpha_i} \exp\left(-\frac{t_i}{t}\right) & \text{for } t \geqslant T_i \end{cases} \quad (2)$$

for both the prompt (the index "$i = p$") γ-ray and initial X-ray decay and for the afterglow("$i = a$"), modeled so that the complete light curve $f_{\rm tot}(t) = f_p(t) + f_a(t)$ contains two sets of four parameters $(T_i, F_i, \alpha_i, t_i)$. The transition from the exponential to the power law occurs at the point $(T_i, F_i e^{-t_i/T_i})$ where the two functional sections have the same value and gradient. The parameter α_i is the temporal power-law decay index and the time t_i is the initial rise timescale.

In previous papers, W07 and Dainotti et al. (2008, 2010) fitted the *Swift* Burst Alert Telescope (BAT)+ X-Ray Telescope (XRT) light curves of GRBs to Equation (2), assuming that the rise time of the afterglow started at the beginning of the decay phase of the prompt emission, T_p, namely $t_a = T_p$. In this paper, we search for an independent measure of the parameters of the afterglow, and thus we leave t_a as a free parameter. In the majority of the cases, we have $t_a \geqslant 0$. We use the redshifts available in the literature (Xiao & Schaefer 2009), on the Greiner Web page http://www.mpe.mpg.de/~jcg/grbgen.html, and in the Circulars Notice arXiv (GCN). (We exclude GRBs with uncertain redshift measurements.) The complete set of GRBs with a definite known redshift until 2011 May is >120, but not all GRBs show a well-defined plateau emission. The fitting procedure fails either when it gives unreasonable values or when the determination of the confidence interval in 1σ does not fulfill the Avni (1976) prescriptions; for more details, see http://heasarc.nasa.gov/xanadu/xspec/manual/XspecSpectralFitting.html. For a proper evaluation of the error bars the latter prescriptions require the computation in the 1σ confidence interval for every parameter, varying the parameter value until the χ^2 increases by 3.5 above the minimum (or the best-fit) value because we are in a tree-parameter space. These rules define the amount that the χ^2 is allowed to increase, which depends on the confidence level one requires and on the number of parameters whose confidence space is being calculated.

The source rest-frame luminosity in the *Swift* XRT bandpass, $(E_{\rm min}, E_{\rm max}) = (0.3, 10)$ keV at time T_a, is computed from the equation

$$L_X(E_{\rm min}, E_{\rm max}, T_a) = 4\pi\, D_L^2(z)\, F_X(E_{\rm min}, E_{\rm max}, T_a) \times K, \quad (3)$$

where $D_L(z)$ is the GRB luminosity distance,[4] F_X is the measured X-ray energy flux, and $K = (1+z)^{-1+\beta_a}$ is the so-called K correction for the X-ray power-law index β_a (Evans et al. 2009; Dainotti et al. 2010). The error bars on the normalization parameter and the slope quoted for L_X and T_a^* are computed using the method of D'Agostini (2005), which is a suitable method where the errors on both variables are comparable (which is the case here) and it is not possible to decide which one is the independent variable to be used in the χ^2 fitting analysis. Moreover, the relation $L_X = aT_a^b$ may be affected by an intrinsic scatter $\sigma_{\rm int}$ of unknown nature that has to be taken into account. Thus, to determine the parameters $(a, b, \sigma_{\rm int})$, we follow the D'Agostini (2005) Bayesian approach and maximize the likelihood function $\mathcal{L}(a, b, \sigma_{\rm int}) = \exp[-L(a, b, \sigma_{\rm int})]$, where

$$L(a, b, \sigma_{\rm int}) = \frac{1}{2}\sum \ln\left(\sigma_{\rm int}^2 + \sigma_{y_i}^2 + b^2\sigma_{x_i}^2\right) + \frac{1}{2}\sum \frac{(y_i - a - bx_i)^2}{\sigma_{\rm int}^2 + \sigma_{y_i}^2 + b^2\sigma_{x_i}^2}, \quad (4)$$

$(x_i, y_i) = (\log L_X, \log T_a)$, and the sum is over the $\mathcal{N}$ objects in the sample. Note that this maximization is actually performed in the two-parameter space $(b, \sigma_{\rm int})$ since a may be estimated analytically as

$$a = \left[\sum \frac{y_i - bx_i}{\sigma_{\rm int}^2 + \sigma_{y_i}^2 + b^2\sigma_{x_i}^2}\right]\left[\sum \frac{1}{\sigma_{\rm int}^2 + \sigma_{y_i}^2 + b^2\sigma_{x_i}^2}\right]^{-1} \quad (5)$$

so that we will not consider it anymore as a fit parameter.

Initially, we had a sample of 116 GRBs with firm redshift, including 11 intermediate class (IC), and with the evaluation of the observables T_a, F_a, and α_a. For some, but not for all of them, we were able to fulfill the Avni prescriptions mentioned above.[5] Among the 116 GRBs, 104 had the proper evaluation of the error measurements, but 3 of them had an error energy parameter $\sigma_E \equiv \sqrt{\sigma_{L_X^*}^2 + \sigma_{T_a^*}^2} > 1$ (for the definition about this parameter and its use, see Dainotti et al. 2011a), and therefore were discarded because such values of the errors have no physical meaning. We thus have a sample of 101 GRBs. To ensure that the inclusion of the IC does not introduce biases into the evaluation of the power slope for the L_X–T_a^* correlation for long GRBs, we checked the slopes of the sample with and without the 8 IC bursts. The two power slopes are compatible within 1σ. We pointed out that in a previous paper (Dainotti et al. 2010) we did not introduce the IC bursts because these represented more than 14% of the sample, while in the current sample they represent only 8%. For the whole sample without the IC, we found a power-law slope of $b = -1.27\pm^{+0.18}_{-0.26}$, while for the whole sample we found $b = -1.32\pm^{+0.18}_{-0.17}$. The Spearman correlation coefficient for the larger sample ($\rho = -0.74$) is higher than $\rho = -0.68$ obtained for a subsample of 66 long-duration GRBs analyzed in Dainotti et al. (2010). The probability of the correlation (of the 101 long GRBs) occurring by chance within an uncorrelated sample is $P \approx 10^{-18}$ (Bevington & Robinson 2003).

Figure 1 (left panel) shows the L_X–T_a^* distribution of 101 GRBs with $0.08 \leqslant z \leqslant 9.4$ and includes afterglows of 93 long and 8 short bursts with extended emission (Norris et al. 2010), called the intermediate class (IC); see Table 1.[6]

[4] We assume a ΛCDM flat cosmological model with $\Omega_M = 0.291$ and $H_0 = 71$ km s^{-1} Mpc^{-1}.

[5] We pointed out here that since this method takes into account the hidden errors, it thus gives greater error estimates than those obtained with the Marquardt–Levenberg algorithm (Marquardt 1963).

[6] For a complete table of the fitting parameters, see http://www.oa.uj.edu.pl/M.Dainotti

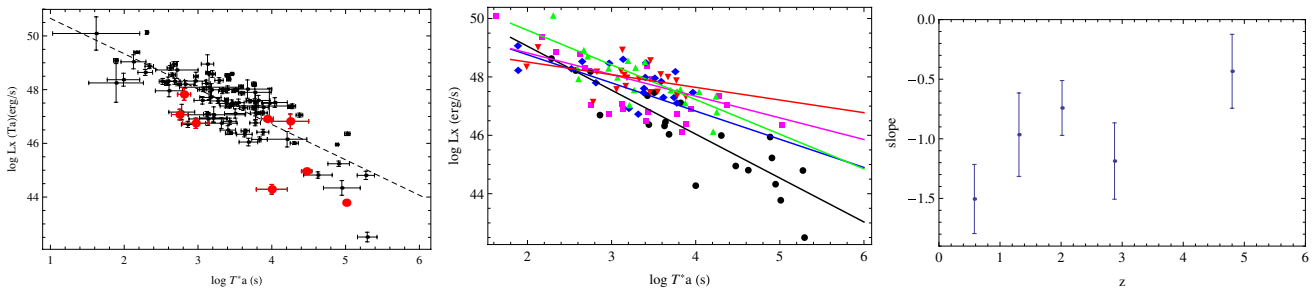

Figure 1. Left panel: L_X vs. T_a^* distribution for the sample of 101 GRB afterglows with the fitted correlation shown by the dashed line. The red points are the IC bursts. Central panel: the same distribution divided into five equipopulated redshift bins shown by different colors—black for $z < 0.89$, magenta for $0.89 \leqslant z \leqslant 1.68$, blue for $1.68 < z \leqslant 2.45$, green for $2.45 < z \leqslant 3.45$, and red for $z \geqslant 1.76$. The solid lines show the fitted correlations. Right panel: the variation of the power-law slope (and its error range) with the mean value of the redshift bins.

(A color version of this figure is available in the online journal.)

Table 1
Fitting Parameters

GRB	z	F_X	dF_X	β_a	$d\beta_a$	$\log T_a^*$	$d \log T_a$	$\log L_X$	$d \log L_X$	Class
50315	1.949	1.16e−11	1.56e−12	1.47	1.23	3.97	0.09	47.49	0.56	Long
50318	1.44	1.0e−8	1.41e−9	0.93	0.18	1.62	0.59	50.09	0.62	Long
50401	2.9	5.41e−11	1.41e−11	0.87	0.23	3.19	0.04	48.58	0.12	Long
050416A	0.6535	2.82e−11	3.82e−12	1.16	0.32	2.86	0.09	46.70	0.11	Long
050505	4.27	4.93e−12	3.84e−12	1.09	0.04	3.67	0.09	48.02	0.34	Long
050525A	0.606	2.92e−9	6.81e−10	1.04	0.15	2.29	0.10	48.84	0.11	Long
050603	2.82	1.10e−12	6.64e−13	0.91	0.10	4.25	0.25	46.82	0.27	IC
50730	3.97	2.58e−11	1.55e−12	0.54	0.05	3.46	0.01	48.58	0.04	Long
50802	1.71	2.20e−11	1.49e−12	0.82	0.08	3.39	0.02	47.63	0.04	Long
050820A	2.612	6.28e−11	5.12e−12	0.91	0.10	3.40	0.03	48.53	0.06	Long
50824	0.83	5.37e−13	1.10e−13	0.95	0.14	4.91	0.15	45.24	0.10	Long
050904	6.29	5.79e−12	6.16e−13	0.61	0.02	3.15	0.40	48.09	0.46	Long
050922C	2.198	8.54e−12	2.29e−12	0.92	0.24	3.38	0.09	47.48	0.16	Long
051016B	0.9364	3.22e−12	5.60e−13	0.83	0.15	3.83	0.11	46.14	0.09	Long
051109A	2.35	2.51e−11	7.74e−12	0.93	0.02	3.40	0.11	48.01	0.13	Long
051221A	0.5465	7.91e−13	1.06e−13	0.95	0.18	4.47	0.07	44.96	0.08	IC
60108	2.03	1.69e−12	2.99e−13	1.00	0.24	3.80	0.09	47.17	0.14	Long
60115	3.53	3.51e−12	6.62e−13	0.96	0.21	3.06	0.11	47.59	0.14	Long
60124	2.297	4.02e−11	3.25e−12	0.97	0.14	3.75	0.03	48.20	0.07	Long
60206	4.05	5.69e−11	1.61e−11	1.29	0.59	3.12	0.08	48.95	0.35	Long
060210	3.91	4.84e−12	2.65e−12	1.05	0.04	3.77	0.22	47.90	0.24	Long
60218	0.0331	1.32e−12	5.34e−13	3.51	0.45	5.29	0.13	42.52	0.18	Long
060223A	4.41	1.14e−11	5.98e−12	1.02	0.12	1.99	0.22	48.37	0.24	Long
60418	1.49	1.47e−10	2.17e−11	1.04	0.22	2.68	0.07	48.30	0.11	Long
060502A	1.51	5.79e−12	5.86e−13	1.04	0.11	3.94	0.08	46.91	0.06	IC
060510B	4.9	3.51e−13	3.96e−14	1.57	0.12	3.78	0.48	47.39	0.5	Long
60512	2.1	1.60e−12	5.69e−13	1.08	0.28	3.31	0.21	46.75	0.20	Long
60522	5.11	1.88e−12	5.80e−13	1.14	0.28	3.17	0.14	47.70	0.21	Long
60526	3.21	4.21e−12	7.22e−13	0.95	0.11	3.27	0.10	47.57	0.09	Long
60604	2.68	2.31e−12	2.92e−13	1.08	0.10	3.87	0.06	47.13	0.07	Long
60605	3.8	6.48e−12	1.03e−13	1.03	0.11	3.32	0.05	47.94	0.09	Long
060607A	3.082	4.17e−12	5.29e−13	0.57	0.06	3.77	0.02	47.53	0.06	Long
60614	0.125	1.54e−12	2.05e−13	0.88	0.05	5.01	0.04	43.79	0.06	IC
60707	3.43	3.74e−12	1.40e−13	1.34	0.18	3.81	0.16	47.59	0.19	Long
60714	2.71	1.71e−11	1.52e−12	0.90	0.15	3.07	0.05	48.01	0.09	Long
60729	0.54	7.97e−12	2.58e−13	1.03	0.04	4.88	0.02	46.95	0.02	Long
60814	0.84	2.75e−11	2.92e−12	1.10	0.11	3.71	0.04	46.96	0.06	Long

Notes. The first column is the GRB identification number; the second, z, the redshift; the third, F_X, the X-ray-observed flux; the fourth, dF_X, the error on the X-ray-observed flux; the fifth, β_a, the spectral index; the sixth, $d\beta_a$, the error on the spectral index; the seventh, $\log T_a^*$, the logarithm of the characteristic rest-frame time; the eighth, $d \log T_a$, the error on $\log T_a$; the ninth, $\log L_X$, the logarithm of the X-ray source luminosity at T_a; the tenth, $d \log L_X$, the error on $\log L_X$; the last column is the class, namely, indication of the GRB type, long or IC (intermediate class).

(This table is also available in a machine-readable form in the online journal.)

However, as mentioned above, since both L_X and T_a^* depend on redshift (L_X increasing and T_a^* decreasing with z) and the sample covers a broad redshift range, all or part of the anti-correlation might be induced by these dependencies. It is therefore important to determine the extent of this effect and determine the true or intrinsic correlation. In addition, any cosmological evolution in L_X and/or T_a^* will affect the degree of the observed anti-correlation. Figure 1 (central panel) shows the color-coded fitted lines. The distribution of the subsamples presents different power-law slopes when we divide the whole

sample into five redshift bins (see Dainotti et al. 2011a for a comparison with a smaller sample) with 20 GRBs in each subsample. The objects in the different bins exhibit some separation into different regions of the L_X–T_a^* plane. The results are shown in Figure 1 (central panel) with the fitted lines. In the right panel of Figure 1, we show the power slope of the redshift bins with the mean values of the redshift bins.

As is evident for each bin, we again found an anti-correlation similar to the whole sample, but the mean values of the slopes are larger (smaller in absolute values), indicating flatter relations, except for the first redshift bin, than for the whole sample. As shown in the right panel of Figure 1 (left), there is some indication that the slope steepens for higher redshifts. This is the first indication that some of the anti-correlation may be induced by the above-mentioned effects.[7] However, in all cases, these differences are all less than 3σ. We expect the correlation slope to be closer to that of the subsamples than the whole sample because each subsample has a smaller redshift range δ_z, which decreases the effect of the redshift dependence and/or redshift evolution. In addition, this test disfavors a strong redshift evolution in the correlation. In the next section, we give a more quantitative analysis of these results using the Efron & Petrosian (EP) method (Efron & Petrosian 1992), which is able to determine the intrinsic correlation among variables in a truncated bivariate distribution.

3. DETERMINATION OF INTRINSIC CORRELATIONS

The first important step for determining the distribution of true correlations among the variables is quantification of the biases introduced by the observational and sample selection effects. In the case under study, the selection effects or biases that distort the statistical correlations are the flux limit and the temporal resolution of the instrument. To account for these effects, we apply the EP technique, which was already successfully applied for GRBs (Petrosian et al. 2009; Lloyd & Petrosian 2000; Kocevski & Liang 2006). Other methodologies for treating selection biases have also been investigated (Collazzi & Schaefer 2008).

The EP method reveals the intrinsic correlation because the method is specifically designed to overcome the biases resulting from incomplete data. Moreover, it also identifies and removes the redshift evolution present in both variables, time and luminosity.

The EP method uses a modified version of the Kendall τ statistic to test the independence of variables in truncated data. Instead of calculating the ranks R_i of all data points among all observed objects, which is normally done for untruncated data, the rank of each data point is determined among its "associated sets," which include all objects that could have been observed given the observational limits. A full discussion of the method is provided in the literature (Singal et al. 2011 and references therein).

Here, we give a brief summary of the algebra involved in the EP method. This method uses the Kendall rank test to determine the best-fit values of the parameters describing the correlation functions, using the test statistic

$$\tau = \frac{\sum_i (\mathcal{R}_i - \mathcal{E}_i)}{\sqrt{\sum_i \mathcal{V}_i}} \quad (6)$$

[7] Note also that as a result, the intercept or normalization parameters a for the individual bins are smaller than the sample as a whole.

to determine the independence of two variables in a data set, say (x_i, y_i) for $i = 1, \ldots, n$. Here, R_i is the rank of variable y for the data point i in its associated set. For untruncated data (i.e., data truncated parallel to the axes), the *associated set* for point i includes all of the data with $x_j < x_i$. If the data are truncated, then the *associated set* must consist only of those points with a lower value of x that would have been observed if they were at the x value of point i given the truncation (see the definition below).

If (x_i, y_i) were independent, then the rank $\mathcal{R}_i$ should be distributed continuously between 0 and 1 with the expectation value $\mathcal{E}_i = (1/2)(i + 1)$ and variance $\mathcal{V}_i = (1/12)(i^2 + 1)$. Independence is rejected at the $n\sigma$ level if $|\tau| > n$. Here, the mean and variance are calculated separately for each associated set and summed accordingly to produce a single value for τ. This parameter represents the degree of correlation for the entire sample when the data truncation is properly accounted for.

Using this statistic, we find the parameterization that best describes the luminosity and time evolution. This means that we have to determine the limiting flux, $F_{\rm lim}$, which gives the minimum observed luminosity for a given redshift, $L_x = 4\pi D_L^2(z) F_X K$ as shown in Figure 2. The nominal limiting sensitivity of XRT, $F_{\rm lim} = 10^{-14}$ erg cm^{-2} s^{-1}, is too low to describe the truncation of our sample (the dashed line). This is because there is a limit in the plateau end times, $T^*_{a,\rm lim} = 242/(1 + z)$ s, see the right panel of Figure 2. Therefore, as pointed out by Cannizzo et al. (2011), this restriction increases the flux threshold to 10^{-12} erg cm^{-2}. Therefore, taking into account the above minimum plateau end time, we have investigated several limiting fluxes to determine a good representative value while keeping an adequate size of the sample. We have chosen the limiting flux $F_{\rm lim} = 1.5\times10^{-12}$ erg cm^{-2}, shown by the red solid line, which allows 90 GRBs in the sample.

3.1. Cosmological Evolutions

The first step required for this kind of investigation is to determine whether the variables L_X and T_a^* are correlated with redshift or are statistically independent of it. For example, the correlation between L_X and the redshift, z, is what we call luminosity evolution, and the independence of these variables would imply the absence of such evolution. The EP method prescribed how to remove the correlation by defining new and independent variables.

Following the approach used for quasars and blazars (Singal et al. 2011, 2013, 2012), we determine the correlation functions $g(z)$ and $f(z)$ when determining the evolution of L_X and T_a^* so that the de-evolved variables $L'_X \equiv L_X/g(z)$ and $T'_a \equiv T_a^*/f(z)$ are not correlated with z. The evolutionary functions are parameterized by the simple correlation functions

$$g(z) = (1 + z)^{k_{Lx}},\ f(z) = (1 + z)^{k_{T_a^*}} \quad (7)$$

so that $L'_X = L_X/g(z)$ refer to the local ($z = 0$) luminosities. This is an arbitrary choice. One can choose any other fiducial redshift by defining $g(z) = [(1 + z)/(1 + z_{\rm fid})]^{k_{Lx}}$. We have also tried this approach, obtaining results that are compatible with those presented. For the source i to obtain the luminosity evolution, the associated set is

$$J_i \equiv \{j : z_j < z_{\rm max}(L_i)\} \vee \{j : L_j > L_i\}, \quad (8)$$

where $z_{\rm max}(L_i)$ is the maximum redshift at which object i with L_j could be placed and still be included in the survey. All of the

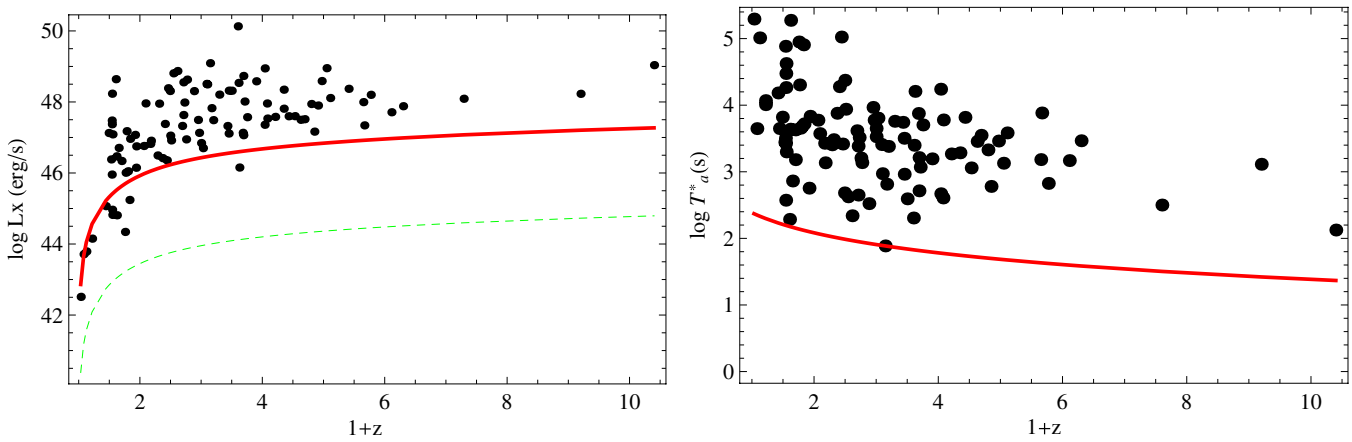

Figure 2. Left panel: the bivariate distribution of L_X and redshift with two different flux limits. The instrumental XRT flux limit 1.0×10^{-14} erg cm^{-2} (dashed green line) is too low to be representative of the flux limit, while 1.5×10^{-12} erg cm^{-2} (solid red line) better represents the limit of the sample. Right panel: the bivariate distribution of the rest-frame time T_a^* and the redshift. The chosen limiting value of the observed end time of the plateau in the sample is $T_{a,\rm lim} = 242$ s. The red line is the limiting rest-frame time, $T_{a,\rm lim}/(1+z)$.

(A color version of this figure is available in the online journal.)

objects in the sample are indicated with i, while the objects in the associated sets are denoted with j. The symbol $\vee$ is intended to represent the union of the sets.

Analogously, to obtain the plateau end-time evolution factor, the associated set for a given object i is

$$J_i \equiv \{j : z_j > z_{\min,i}\} \vee \{j : T_j > T_i\}, \quad (9)$$

where $z_{\min}(T_{a_i})$ is the minimum redshift at which object i could be placed and still be included in the survey given its plateau duration and the limiting time of the observation.

Using the specialized version of Kendell's τ statistic, the values of k_{L_x} and $k_{T_a^*}$ for which $\tau_{L_x} = 0$ and $\tau_{T_a^*} = 0$ are those that best fit the luminosity and plateau end-time evolution, respectively, with the 1σ range of uncertainty given by $|\tau_x| \leqslant 1$. Plots of τ_{L_x} and $\tau_{T_a^*}$ versus k_{L_x} and $\tau_{T_a^*}$ are shown in Figure 4. With k_{L_x} and $k_{T_a^*}$, we are able to determine the de-evolved observables T'_a and L'_X.

We evidence that there is no discernable luminosity evolution, $k_{L_x} = -0.05^{+0.35}_{-0.55}$, but there is a significant evolution in T_a^*, $k_{T_a^*} = -0.85^{+0.30}_{-0.30}$.

3.2. Intrinsic LT Correlation

This is the first time the EP method has been applied in a parameter space for a bivariate correlation that involves a luminosity and a time, while previously the EP applications have been done in a luminosity–luminosity space (Singal et al. 2012). Therefore, we stress that this means different trends in the data truncation, as we have shown in Figure 2. In the $[L_X - T_a^*]$ variable space, we apply the EP method to define the associated sets as

$$J_i \equiv \{j : L'_{\min}(z_j) < L'(z_i)\} \vee \{j : L'_j > L'_i\} \vee \{j : T'_{a_{\min}}(z_j) < T'_a(z_i)\}, \quad (10)$$

where $L'_{\min}(z_j)$ and $T'_{a_{\min}}(z_j)$ are, respectively, the de-evolved minimum luminosity and de-evolved plateau time at redshift z_j that object j could have and still be included in the survey given the flux limits, its redshift, and the limiting time of the observation: $L_{\min}(z_j) = 4\pi D_L^2(z_j) F_{\rm lim} K$ and $T^*_{a_{\min}}(z_j) = T_{a,\rm lim}/(1+z_j)$. Using the Kendall τ rank test, we determine whether L_X and T_a^* are independent or not. The test shows some dependence, so we apply a coordinate transformation by defining a new luminosity L'_X as

$$\log_{10} L'_X = \log L_x + \alpha \log T_a^*. \quad (11)$$

We then vary α and determine the value of τ (the correlation between L'_X and T'_a) as a function of α. The value of α which gives $\tau_\alpha = 0$ determines the correlation between L_X and T_a^* with the 1σ range of uncertainty given by $|\tau_\alpha| \leqslant 1$.

Figure 3 shows the variation of $\tau_{\rm alpha}$ with α. As can be seen, independence is achieved ($\tau = 0$) for $\alpha = 1.07$ with a 1σ range of $\alpha = (-1.21, -0.98)$, therefore $\alpha = -1.07^{+0.09}_{-0.14}$. This means that L_X and T_a^* are correlated with an intrinsic slope of 1.07 and that the significance of this correlation is at the 12σ level. The α value is flatter than that obtained from the raw data of the whole sample (parameter b) and it is compatible with the average value of the slopes of the subsamples shown in Table 1.

With the EP method, we are able to both overcome the problem of selection effects and determine the intrinsic value of the slope because we removed the induced correlation from the observables due to the time evolution and luminosity evolution dividing the respective time and luminosity for the respective evolution functions, as is explained above. Any differences between the correlation obtained from our methods and the present one in the raw data are assumed to arise from selection effects and partly to time evolution. The evolution seen in Figure 1 (central panel) is due to observational biases and partly to time evolution. In fact, we have determined that there is no cosmological evolution of L_X, and that the evolution of T_a^* becomes significant at high redshift only.

We also present results for a sample of 53 GRBs that are in common between a previous sample of 77 GRBs (Dainotti et al. 2010) and the present one (see the green line of Figures 3 and 4). For the sample of 53 GRBs, we have adopted as a limiting flux 1.8×10^{-12} erg cm^{-2} s^{-1}, adopting the same criterion as for the larger sample. In this case, we have 47 GRBs remaining above the adopted flux limit, again resulting in 90% of the sample being retained. We note that there is compatibility within the 1σ range among the power-law slopes (α) of the two samples. The two samples are fitted with different fitting procedures, one procedure leaves t_a free to vary (101 sample)

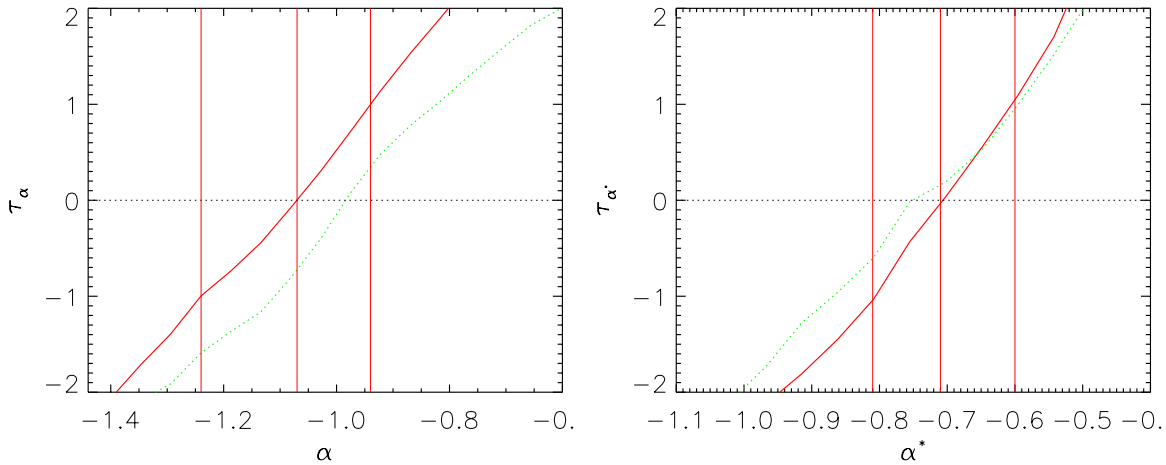

Figure 3. Left panel: test statistic τ vs. α, the slope of the LT correlation. Right panel: test statistic τ vs. $\alpha^* = 1/\alpha$, the power slope of the reciprocal of the LT correlation defined by Equation (12). The vertical lines show the best value $\tau = 0$, and the 1σ range for $|\tau| \leqslant 1$ for α and α^*. Note that we expect $\alpha = 1/\alpha^*$, which is the case within 1σ, showing the consistency of our results. The τ values for the earlier sample of 53 GRBs are also shown by (green) dotted lines. This is also consistent with the result from the current sample of 101 GRBs.

(A color version of this figure is available in the online journal.)

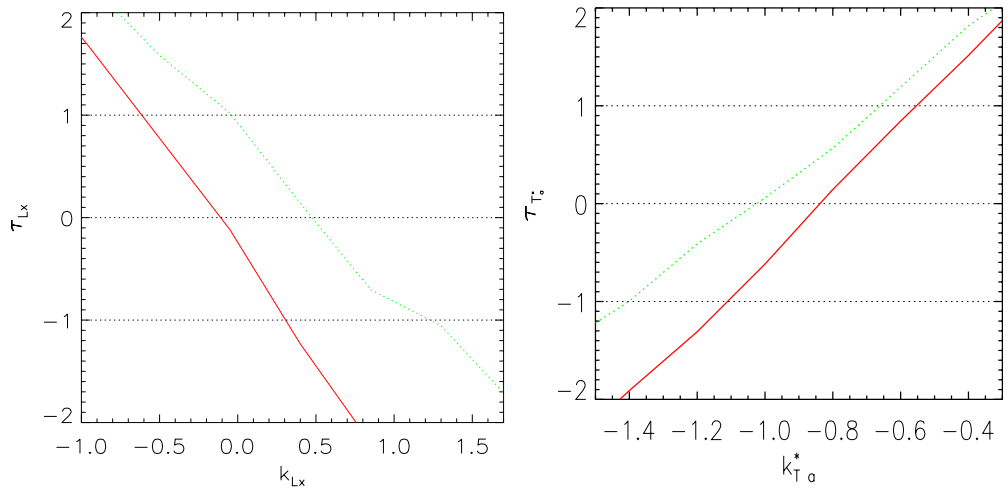

Figure 4. Left panel: test statistic τ vs. k_{L_x}, the luminosity evolution defined by Equation (8). Right panel: test statistic τ vs. $k_{T_a^*}$, the time evolution defined by Equation (9). The red line represents the full sample of 101 GRBs, while the green line represents the small sample of 47 GRBs in common with the previous sample of 77 GRBs.

(A color version of this figure is available in the online journal.)

and the other fixes $t_a = T_p$, where T_p is the beginning of the decay phase of the prompt emission; therefore, we here stress that we still find compatible results proving that the LT correlation intrinsic slope is independent of the particular procedure adopted.

In addition, for a consistency check we have used an inverted transformation

$$\log_{10}(T_a') = \log T_a^* + \alpha^* \log L_X \tag{12}$$

and followed the same procedure to determine τ as a function of α^*. We expect $\alpha^* = 1/\alpha$. The result is shown in the lower right panel of Figure 7. Values of $\alpha^* = -0.71^{-0.10}_{+0.12}$ are compatible within 2σ with $1/\alpha = -0.93 \pm 0.09$ obtained from the previous transformation. This further demonstrates that the method is well built and the results are robust. However, for an exact compatibility we would expect $\alpha^* = 1/\alpha$ (see also the Appendix).

4. THE CUMULATIVE LOCAL LUMINOSITY AND DENSITY FUNCTIONS

Since we found no luminosity evolution, the cumulative distribution of $\Phi(>L) = \int_L^\infty \Psi(L')dL'$ according to our method (Petrosian 1992) is given as

$$\Phi_i(L_i) = \prod_k \left(1 + \frac{1}{n(k)}\right). \tag{13}$$

Here, $n(k)$ is the number of objects in the associated sets of object k, namely, those with $L > L_k$ and $z < z_{\max}$.

The density rate evolution $\rho(z)'$ and the luminosity function (with $'$ we indicate the differential symbol), which give the number of objects per unit comoving volume V per unit source luminosity, can be computed using the EP method. The method gives the cumulative functions $\sigma(< z)' = \int_0^z \rho(z')\,[dV(z')/dz']\,dz'$ and $\phi(>L') = \int_{L'}^\infty \psi(L'')\,dL''$. The differential functions ρ' and ψ are obtained by differentiation.

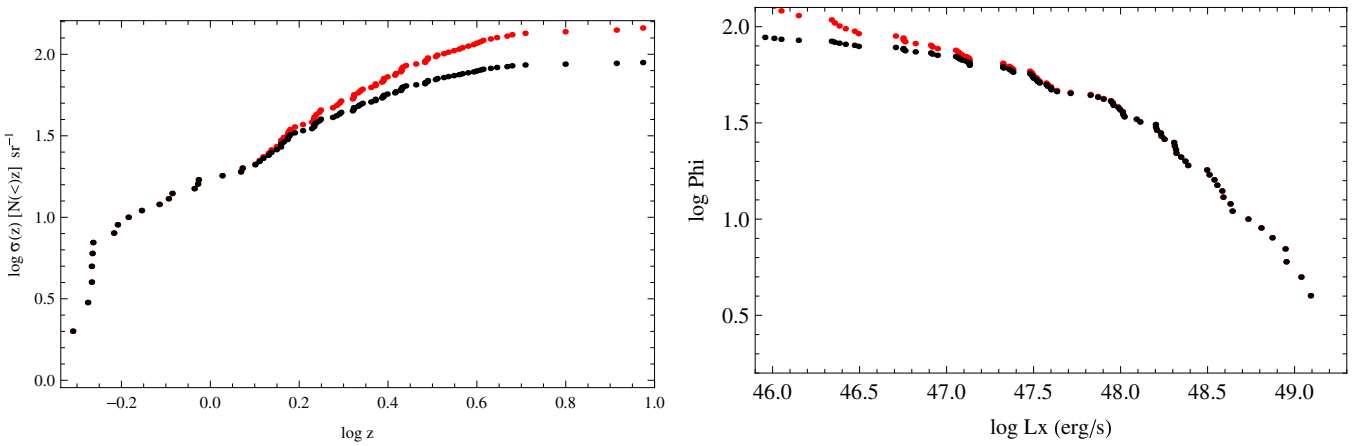

Figure 5. Left panel: the cumulative redshift distribution, $N(> z)$, of the raw data (black points) and the cumulative distribution, $\sigma(z)$, corrected by the EP method (red points) and described in Section 4. Right panel: the cumulative local luminosity distribution of the raw data (black point) and corrected by the EP method (red points).

(A color version of this figure is available in the online journal.)

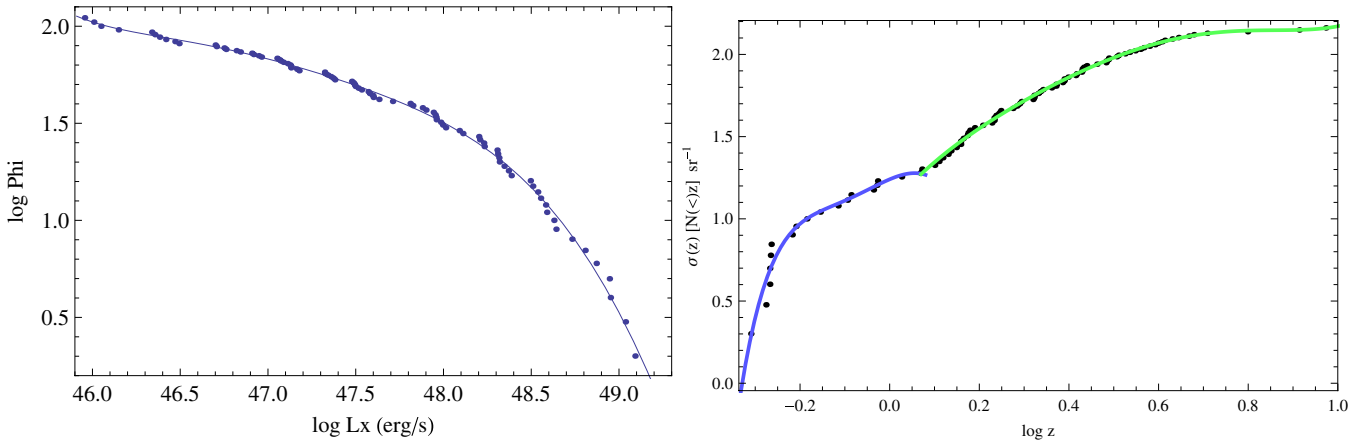

Figure 6. Left panel: the cumulative intrinsic luminosity function determined by the EP method along with a fitted function as discussed in Section 4. Right panel: the cumulative intrinsic density distribution with two fitted function lines as discussed in Section 4. The blue line is until $z = 1$, while the green line is for $z > 1$.

(A color version of this figure is available in the online journal.)

One can define the cumulative density function as follows:

$$\sigma(z_j) = \prod_i \left(1 + \frac{1}{m(i)}\right), \tag{14}$$

where i runs over all objects with a redshift lower than or equal to z, and $m(i)$ is the number of objects with a redshift lower than the redshift of object i *which is in object j's associated set*. In this case, the associated set is again those objects with an X-ray luminosity that would be seen if they were at object i's redshift. The use of only the associated set for each object removes the biases introduced by the data truncation. We show the distribution of the corrected cumulative density distribution in the right panel of Figure 5 (red points), which is contrasted with the raw distribution (black points).

As is evident, the correction for the cumulative density starts to apply for $z = 1$, namely, we have a higher density of GRBs than that observed for $z > 1$. In Figure 5 (left panel), the corrected cumulative luminosity function agrees with the raw observed luminosity distribution until $L_X = 10^{48}$ erg s^{-1}, while for higher values of the luminosity the two distributions separate.

To obtain the differential distribution $\psi(L)$ and $\rho'(z)$, we fitted the cumulative luminosity function with a polynomial of the order of seven, while for the cumulative density we divide the distribution into two parts, one with $z \leqslant 1$, as we can see from Figure 6, (blue line) and the other part for $z \geqslant 1$ (green line). The two fitting lines are both a polynomial of the order of five.

5. DISCUSSION

The obtained τ_α versus α plot (right panel of Figure 3) clearly demonstrates the existence of a significant LT correlation at the 12σ level, characterized by the value found for the power-law slope relating the luminosity and the plateau end times.

Therefore, the analysis presented, with the intrinsic value of the power-law slope of the LT correlation, provides new constraints for physical models of GRB explosion mechanisms. With this new determination of the correlation power-law slope, we discuss the consequences of these findings for GRB physical models. The LT relation is predicted by several theoretical models (Cannizzo & Gehrels 2009; Cannizzo et al. 2011; Dall'Osso 2010; Yamazaki 2009; O'Brien & Rowlinson 2012; Bernardini et al. 2012a) and in other observational ones (Ghisellini et al. 2009; Qi & Lu 2012), proposed for the physical GRB evolution in the time T_a. Recently, Oates et al. (2012) pointed out the

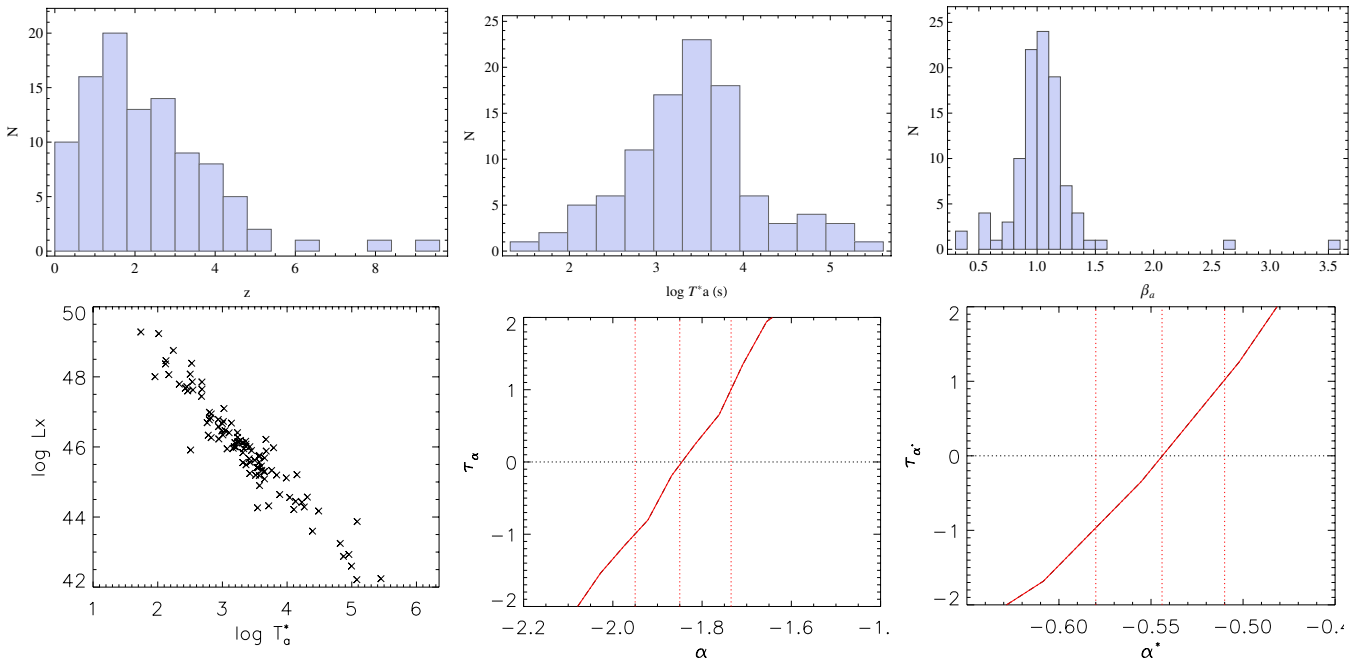

Figure 7. Upper panels: the distribution of the redshift (left), the time T_a^* (middle), and the spectral index (right) for the sample of 101 GRBs used in the analysis. Lower panels: the L_X–T_a^* distribution for a set of 101 simulated GRBs discussed in the Appendix (left); test statistic τ vs. the LT correlation power slope parameter α (center); and the reciprocal of it α^* (right), for the simulated set. The 1σ range of best-fit values is where $|\tau| \leqslant 1$, shown by the vertical dotted lines.
(A color version of this figure is available in the online journal.)

existence of an anti-correlation between the luminosity at 200 s and the decay slope of the optical light curve. This correlation is related to the LT one considered here. Racusin & Oates (2013) recover the Oates et al. correlation in the X-ray band. Therefore, it is now even more challenging to understand the meaning of the L_X and T_a^* correlation, which becomes the principal X-ray afterglow correlation from which further correlations in other wavelengths can be derived. From a theoretical point of view, the Cannizzo model predicts a correlation slope (3/2) that is only in agreement with our intrinsic correlation power law within 3σ, while the model of Yamazaki predicts a less steep decay that is in agreement within 1σ with the presented results. The LT correlation is also recovered for short GRBs (O'Brien & Rowlinson 2012) within the magnetar scenario. Any physical interpretation of the LT correlation should be based on the intrinsic power slope and not that obtained from the raw observed quantities. In fact, assuming the observed power law as a key feature to discriminate among physical models could lead to misleading results based either on data truncation or on redshift evolution. We conclude that determining the intrinsic correlations among, and distributions of, the observables is a necessary step before any possible and plausible use of the LT correlation as a theoretical model discriminator, distance estimator, and useful cosmological tool. Therefore, this paper opens a new perspective not only on the interpretation of the LT correlation, but also on the other existing GRB correlations and prepares for a new possible future approach for the use of GRBs in cosmology.

This work made use of data supplied by the UK Swift Science Data Centre at the University of Leicester. M.D. is grateful to Richard Willingale and Paul Obrien for comments on the paper and Qin Rong Chen for fruitful discussions. M.D. is also grateful to the Polish MNiSW through grant No. N203 579840, the Fulbright Scholarship, and the Ludovisi-Blanceflor Foundation. M.O. is grateful to the Polish National Science Centre through grant DEC-2012/04/A/ST9/00083.

APPENDIX

As a further test of the robustness of the main conclusion of this work, we have applied the analysis methods discussed here to a simulated observational data set with a known intrinsic LT correlation. As is clear from the upper panels of Figure 7, the distributions of the three observables in the real data, the time, T_a^*, the spectral index, β_a, and the redshift, z, can be approximated with normal distributions with mean values of $\langle\beta_a\rangle = 1.05$, $\langle T_a^*\rangle = 3.5$, and $\langle z\rangle = 2.09$. Therefore, we have created a Monte Carlo population with these distributions. The luminosities are determined by applying an LT correlation with $\log L_X \approx -1.9 \log T_a^*$, where -1.9 in this case is the imposed α slope of the LT correlation (see the lower left panel of Figure 7). We then compute the simulated fluxes from the simulated β, z, and L_X. We have imposed the same limiting flux used for the real observational data to form an "observed" simulated data set to which we then apply the analysis method discussed in this work. Application of the method successfully recovers the known intrinsic power-law slope of the LT correlation and its inverse as is shown in the lower central and right panels of Figure 7.

REFERENCES

Amati, L., Frontera, F., & Guidorzi, C. 2009, A&A, 508, 173
Avni, Y. 1976, ApJ, 210, 642
Bernardini, M. G., Margutti, R., Mao, J., Zaninoni, E., & Chincarini, G. 2012a, A&A, 539, A3
Bernardini, M. G., Margutti, R., Zaninoni, E., & Chincarini, G. 2012b, MNRAS, 425, 1199
Bevington, P. R., & Robinson, D. K. 2003, Data Reduction and Error Analysis for the Physical Sciences (3rd ed.; New York: McGraw-Hill)
Butler, N. R., Kocevski, D., & Bloom, J. S. 2009, ApJL, 694, L76

Cabrera, J. I., Firmani, C., Avila-Reese, V., et al. 2007, MNRAS, 382, 342
Cannizzo, J. K., & Gehrels, N. 2009, ApJ, 700, 1047
Cannizzo, J. K., Troja, E., & Gehrels, N. 2011, ApJ, 734, 35
Cardone, V. F., Capozziello, S., & Dainotti, M. G. 2009, MNRAS, 400, 775
Cardone, V. F., Dainotti, M. G., Capozziello, S., & Willingale, R. 2010, MNRAS, 408, 1181
Collazzi, A. C., & Schaefer, B. E. 2008, ApJ, 688, 456
Cucchiara, N., Levan, A. J., Fox, D. B., et al. 2011, ApJ, 736, 7
D'Agostini, G. 2005, arXiv:physics/0511182
Dainotti, M. G., Cardone, V. F., & Capozziello, S. 2008, MNRAS, 391, L79
Dainotti, M. G., Cardone, V. F., Capozziello, S., Ostrowski, M., & Willingale, R. 2011a, ApJ, 730, 135
Dainotti, M. G., Ostrowski, M., & Willingale, R. 2011b, MNRAS, 418, 2202
Dainotti, M. G., Willingale, R., Cardone, V. F., Capozziello, S., & Ostrowski, M. 2010, ApJL, 722, L215
Dall'Osso, S., Stratta, G., Guetta, D., et al. 2011, A&A, 526A, 121
Efron, B., & Petrosian, V. 1992, ApJ, 399, 345
Evans, P., Beardmore, A. P., Page, K. L., et al. 2009, MNRAS, 397, 1177
Fenimore, E. E., & Ramirez-Ruiz, E. 2000, ApJ, 539, 712
Ghirlanda, G., Ghisellini, G., & Firmani, C. 2006, NJPh, 8, 123
Ghirlanda, G., Ghisellini, G., & Lazzati, D. 2004, ApJ, 616, 331
Ghisellini, G. 2008, in AIP Conf. Proc. 1065, 2008 Nanjing Gamma-Ray Burst Conference, ed. Y. F. Huang, Z. G. Dai, & B. Zhang (Melville, NY: AIP), 137
Ghisellini, G., Nardini, M., Ghirlanda, G., & Celotti, A. 2009, MNRAS, 393, 253
Izzo, L., Pisani, G. B., Muccino, M., et al. 2013, EAS, 61, 595
Kocevski, D., & Liang, E. 2006, ApJ, 642, 371
Lloyd, N., & Petrosian, V. 1999, ApJ, 511, 550
Lloyd, N., & Petrosian, V. 2000, ApJL, 543, L722
Marquardt, D. 1963, SIAM J. Appl. Phys., 11, 431
Nemmen, R. S., Georganopoulos, M., Guiriec, S., et al. 2012, Sci, 338, 1445
Norris, J. P., & Bonnell, J. T. 2010, ApJ, 717, 411
Norris, J. P., Marani, G. F., & Bonnell, J. T. 2000, ApJ, 534, 248
Oates, S. R., Page, M. J., & De Pasquale, M. 2012, MNRAS, 426, 86
O'Brien, P. T., & Rowlinson, A. 2012, in IAU Symp. 279, Death of Massive Stars: Supernovae and Gamma-Ray Bursts, ed. P. W. A. Roming, N. Kawai, & E. Pian (Cambridge: Cambridge Univ. Press), 297
O'Brien, P. T., Willingale, R., Osborne, J., et al. 2006, ApJ, 647, 1213
Petrosian, V. 1992, in Statistical Challenges in Modern Astronomy, ed. E. D. Feigelson & G. H. Babu (New York: Springer), 173
Petrosian, V. 1998, ApJ, 507, 1
Petrosian, V. 1999, in IAU Symp. 194, Active Galactic Nuclei and Related Phenomena, ed. Y. Terzian, D. Weedman, & E. Khachikian (San Francisco, CA: ASP), 105
Petrosian, V. 2002, in ASP Conf. Proc. 284, AGN Surveys, Proc. IAU Colloquium 184, ed. R. F. Green, E. Ye. Khachikian, & D. B. Sanders (San Francisco, CA: ASP), 389
Petrosian, V., Bouvier, A., & Ryde, F. 2009, arXiv:0909.5051
Postnikov, S., Dainotti, M. G., Hernandez, X., & Capozziello, S. 2013, ApJ, submitted
Qi, S., & Lu, T. 2012, ApJ, 749, 99
Racusin, J., & Oates, S. 2013, HEAD, 1312725R
Rowlinson, A., O'Brien, P. T., Metzger, B. D., Tanvir, N. R., & Levan, A. J. 2013, MNRAS, 430, 1061
Sakamoto, T., Hill, J., Yamazaki, R., et al. 2007, ApJ, 669, 1115
Schaefer, B. E. 2003, ApJL, 583, L67
Shahmoradi, A., & Nemiroff, R. J. 2009, in AIP Conf. Proc. 1133, Gamma-Ray Burst: Sixth Huntsville Symposium, ed. C. Meegan, C. Kouveliotou, & N. Gehrels (Melville, NY: AIP), 425
Singal, J., Petrosian, V., & Ajello, M. 2012, ApJ, 753, 45
Singal, J., Petrosian, V., Lawrence, A., & Stawarz, Ł. 2011, ApJ, 743, 104
Singal, J., Petrosian, V., Stawarz, L., & Lawrence, A. 2013, ApJ, 764, 43
Sultana, J., Kazanas, D., & Fukumura, K. 2012, ApJ, 758, 32
Xiao, L., & Schaefer, B. E. 2009, ApJ, 707, 387
Yamazaki, R. 2009, ApJL, 690, L118
Yonetoku, D., Murakami, T., Nakamura, T., et al. 2004, ApJ, 609, 935
Yu, B., Qi, S., & Lu, T. 2009, ApJL, 705, L15
Willingale, R. W., O'Brien, P. T., Osborne, J. P., et al. 2007, ApJ, 662, 1093